RSC Advances

ROYAL SOCIETY OF CHEMISTRY

www.rsc.org/advances

Journal Name

ARTICLE

Towards efficient biocatalysts: photo-immobilization of a lipase on novel lysozyme amyloid-like nanofibrils

Received 00th January 20xx,
Accepted 00th January 20xx

DOI: 10.1039/x0xx00000x

www.rsc.org/

Silvina Chaves,[a] Licia M.Pera,[b] Cesar Luis Avila,[a] Cintia M.Romero,[b] Mario Baigori,[b] F. Eduardo Morán Vieyra,[c] Claudio D. Borsarelli,[c] and Rosana N. Chehin[a]*

Herein, we report the preparation and characterization of a new biocatalyst based on the photo-immobilization of a lipase onto hybrid protein:sugar nanofibrils. The nanofibrils are obtained through the aggregation of hen white egg lysozyme induced by the highly sulfated glycosaminoglycan heparin. The new hybrid nanomaterial could be easily functionalized using photochemical reaction to attach lipases through dityrosine covalent bonds. Compared to the free enzyme, the photo-immobilized lipase has better thermostability and enhanced resistence to non-conventional environment. Structural and morphological characterization of the nanofibrils shows that they are compatible with amyloid-like aggregates. In addition, the supramolecular arrangement of heparin and lysozyme within the building unit of the nanofibrils is also proposed. The procedure reported herein could be useful to design a new generation of insoluble biocatalyst by a single photo-click step which is definitely cleaner and faster than conventional chemical cross-linked procedures.

Introduction

Enzyme catalysts show an increasing application in technological processes as alternatives to traditional chemical catalysts, and their development is strongly driven by its profitability and eco-efficiency. Of all industrially important enzymes, lipases (triacyglycerol acylhydrolases EC 3.1.1.3) are exploited to a full extent due to their capability to catalyze a variety of reactions such as hydrolysis, esterification and transesterification. On the other hand, the lipase immobilization has proved to be a powerful tool for tuning its catalytic properties such as stability, specificity or activity.[1, 2] Thus, the improvement of the lipase behavior has been successfully applied for the synthesis of polymers, biodiesel and enantiopure compounds.[3-5]

Immobilization is usually required for the use of an enzyme as an industrial biocatalyst, and is the simplest solution to the solubility problem of these interesting biocatalysts. Although there are many established immobilization protocols[6, 7] the search of new enzyme immobilization techniques, as a complementary approach to genetic engineering, are constantly pursued to obtain efficient biocatalysts. For example, Verma *et al*[8] proved the effect of the immobilized lipase on carbon nanotubes (MWNTs) functionalised with amino group while other authors proved the lipase immobilization on Chitosan TiO2.[9] These supports were effective for lipase immobilization but until now, only some reports have been written about biological or biocompatible nanotube supports.[10]

An interesting strategy which can be applied is the enzyme incorporation on nanostructured materials in order to establish suitable microenvironments for both hydrolytic and synthetic reactions.[11] Therefore discovering novel bionanomaterials capable of immobilizing enzymes, improving their activity, and allowing them to be used again is essential in biocatalytic processes. In this sense, amyloid fibrils belong to the group of ordered nanostructures that are self-assembled in controlled environmental conditions with increasing applications to be exploited by industry, research and medicine.[12, 13]

Amyloid aggregates are insoluble, several hundred nanometers long, relatively straight and branchless nanostructures that nearly any protein can self-assemble into,[14] with the cross-β motif as a common structural feature.[15] The architecture of the hallmark cross-β motif can show variations in response to changes in the fibril growth conditions[16] or the primary amino acid sequence of the protein.[17-19] There are two major tracks that have been identified to describe the mechanism by which proteins change from their soluble native state into amyloid aggregates: a) exposure of aggregation prone peptide as a consequence of protein unfolding due to changes in the local environmental conditions that start the aggregation process resulting into canonical amyloid fibrils i.e a set of β-sheets parallel to the fibril axis, with their strands perpendicular to this axis,[17] and b) fibrillar structure where the native or native-like protein conformation is mainly kept and the transitions across the unfolding state is

[a] *Instituto Superior de Investigaciones Biológicas (INSIBIO), CONICET-UNT, and Instituto de Química Biológica "Dr. Bernabé Bloj", Facultad de Bioquímica, Química y Farmacia, UNT. Chacabuco 461, T4000ILI – San Miguel de Tucumán, Argentina.*
[b] *Planta Piloto de Procesos Industriales Microbiológicos (PROIMI-CONICET), Av. Belgrano y Pasaje Caseros, T4001 MVB, San Miguel de Tucumán, Tucumán, Argentina. Facultad de Bioquímica, Química, Farmacia, Universidad Nacional de Tucumán, Ayacucho 471, T4000INI, San Miguel de Tucumán, Tucumán, Argentina.*
[c] *Instituto de Bionanotecnología, INBIONATEC- CONICET. Universidad Nacional de Santiago del Estero (UNSE). RN 9, Km 1125. G4206XCP, Santiago del Estero, Argentina.*

† Footnotes relating to the title and/or authors should appear here.
Electronic Supplementary Information (ESI) available: [details of any supplementary information available should be included here]. See DOI: 10.1039/x0xx00000x

absent. Such supramolecular arrangements are currently referred to as amyloid-like aggregates.[20, 21] Both, amyloid and amyloid-like fibrils share some characteristics including: morphology; binding of the flat-shape dyes Congo red and thioflavin T; the characteristic green–yellow birefringence of Congo red and unusual stability.[22] In fact, the amyloid supramolecular arrangements with its extensive hydrogen bond network and side-chain interactions is responsible for such extraordinary structural resistance over a wide range of pH, salt concentrations, high pressure, proteolysis and dehydration.[23-25] In the last few years, an increasing interest has been focused on amyloid fibrils, not only from the medical and health care field point of view but also from their use as new bionanomaterials for emerging applications, finding its origins in the highly organized nanoscale structures, regularity, multifunctionality, stability and extraordinary mechanical properties of the resulting fibrils.[26-28] In fact, these biomaterials have been proposed as new scaffolds to enzyme immobilization. The main feature that makes it an ideally functionalized nanoscaffold is its amino acidic constitution, which can allow side-chain functionalization or reactions for those solvent exposed residues.

Hen Egg-White Lysozyme (HEWL) has been widely used to study the mechanism of amyloid aggregation *in vitro.*[29] This protein is homologous to human lysozyme, which has been shown to form amyloid fibrils, involved in hereditary systemic amiloidosis.[30] Amyloid aggregates of HEWL obtained in vitro under unfolding conditions have similar morphological properties to those extracted from pathological deposits.[31] In this way, HEWL amyloid fibrils were obtained at pH 2.0,[32] in the presence of trifluoroethanol,[33] ethanol[34] or guanidine hydrochloride.[35] It has also been reported that the reduction of the four disulfide bonds in HEWL can cause amyloid fibrils formation.[36] Recent reports show that negatively charged lipid membranes trigger HEWL amyloid-like fiber formation at low lipid-to-protein molar ratio under physiological temperature and pH conditions, albeit that any cross-β was detected in these nanostructures.[37]

In the present work, we used heparin, a highly sulfated glycosaminoglycan, to induce the HEWL aggregation obtaining amyloid-like nano fibrils without the addition of any chaotropic agent, solvent, extreme pHs, or high temperature treatments. The method proposed herein yields stable nano fibrils with a supra molecular arrangement where HEWL: heparin complex is proposed. These nano-fibrils have the typical cross-β motif as detected by both fluorescence and infrared spectroscopy with a considerable decrease of the aggregation times as compared to the precedent protocols. These insoluble heparin-induced amyloid-like fibrils were used as novel class of nano-support for lipase enzyme covalent immobilization exploding the functional groups from the exposed amino acids residues through a photo-induced cross-linking reaction.[38, 39] The resulting insoluble nano-sized biocatalyst showed an enzyme stability higher than the soluble enzyme under several extreme conditions, indicating the suitable combination of the click chemistry[40] with this new nanostructure in order to obtain an efficient nano-sized biocatalyst with potential application in biotechnological processes.

Results and discussion

Formation of heparin-induced HEWL amyloid-like fibrils: the ability of heparin to induce HEWL aggregation was monitored by the classical ThT fluorescence assay, which binds to cross β-sheets structures that are the hallmark in amyloid fibril structure.[41] In the absence of heparin, HEWL aggregation was not significantly detected in neutral HEPES buffer at 37 °C (Figure 1a), suggesting that the enzyme remains in its native state. On the contrary, heparin addition induced a rapid increase in ThT fluorescence at 482 nm without any measurable lag time. The undetectable lag phase in ThT fluorescence emission after heparin addition was also observed for other proteins like α-synuclein[42] and GAPDH.[43] Fluorescence rise-time was almost independent from the amount of added heparin and the final fluorescence intensity of ThT was increased with heparin concentration, suggesting that the amount of cross-β structures formed is proportional to the amount of added polysaccharide. To confirm that the observed ThT fluorescence increments were produced by the formation of larger size aggregated species, the second-order light scattering at 600 nm observed upon excitation at 300 nm was also monitored.[43, 44] The lifetime τ_β obtained by first-order growth fitting of the intensity of scattered light was similar to that obtained by monitoring of ThT fluorescence of the HEWL:heparin mixtures (Figure 1b). This result suggests that heparin efficiently induced the formation of larger sized particles with cross-β structure at 37 °C and pH 7.4. The SEM images of Figures 1c and 1d show the final morphologies of the aggregate species formed after incubation for 5 days at 37 °C and pH 7.4 without and with the addition of heparin, respectively. Only in the presence of heparin well-shaped nano-fibrils (≈300 nm width× 13μm length) were formed, in accordance with the previous spectroscopic results.

One of the main features in enzyme immobilization is related to the lack of biological activity of the support in order to avoid any interference. HEWL is also referred as muramidase due to its activity on bacterial cell wall,[45] as well as a membrane disrupter in cell-free system.[46] In this way, it has proved essential to learn whether after the formation of amyloid aggregate, the muramidase and the membrane permeabilization activities are prevalent in the protein. Figure 1e shows the muramidase activity of 1/10 dilution of 1 mg/ml HEWL on *Micrococcus lysodecticus* alone or in the presence of 0.750 mg/ml heparin. The exponential decreases of absorbance measured at 540 nm of the bacterial suspension indicates that the muramidase activity measured for the native protein is in good agreement previous report.[47] On the contrary, after 1 h of incubation of heparin-HEWL sample, the muramidase activity showed a significant reduction, due to the progressive incorporation of monomeric HEWL into the supramolecular aggregates formed with heparin. In fact, after 1 day incubation, the membrane activity of HEWL was completely lost. The previous result was also obtained with HEWL:heparin sample after 5 days of preincubation. These results strongly suggest that only monomeric HEWL shows muramidase activity, while the HEWL: heparin nano fibrils as well as the heparin alone are completely inactive.

In addition, the effect of the HEWL aggregation on acidic membrane permeability was studied by using fluorescence techniques. Figure 1F shows the fluorescence increases of pre-encapsulated self-quenched calcein in small unilamellar vesicles (SUV) of phosphatidylcholine:phosphatidic acid (8:2). In the absence of heparin, the native HEWL is capable to induce changes on the lipid membrane permeability, as measured by calcein fluorescence increases,as previously reported.[48] However, in the presence of

heparin, the HEWL activity in membrane leakage was progressively reduced with the incubation time. As observed for the murasidase activity, the SUV membrane permeability is only increased by monomeric HEWL since heparin alone did not induce any permeability change to the SUV.

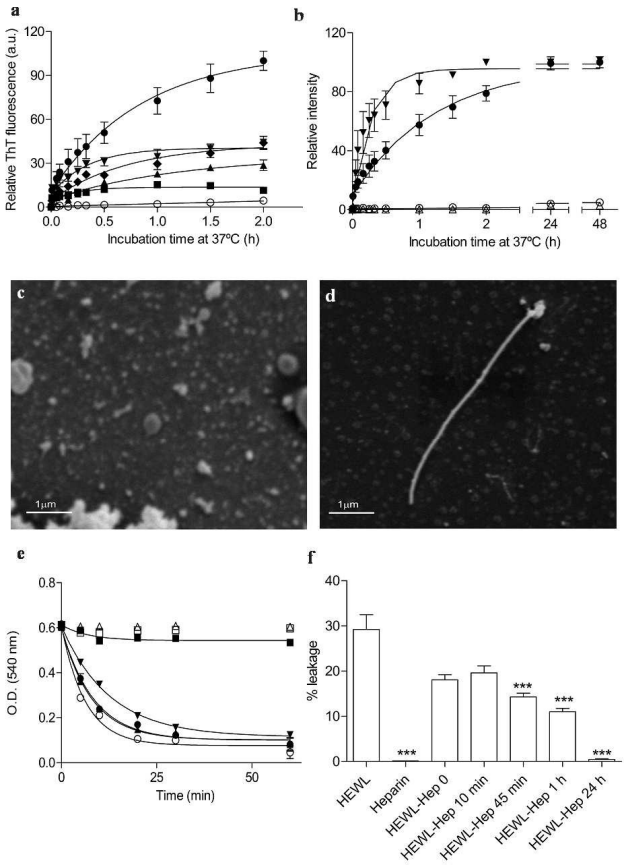

Figure 1 (a) HEWL aggregation kinetics measured by thioflavin T fluorescence emission. 0.1 mg/ml HEWL alone (○), or in the presence of 0.050(■), 0.060(▲), 0.070(▼), 0.075(●) and 0.100 mg/ml (♦) of heparin. **(b)** Variation of the second-order scattering intensity at 600 nm (i.e. λ_{ex}=300 nm) during the aggregation process. HEWL, alone (△) and in presence of 0.075 mg/ml of heparin (▼), and ThT fluorescence emission of HEWL alone (○) or in presence of heparin 0.75 mg/ml (●). **(c)** and **(d)** VP–SEM images of HEWL (1mg/ml) in the absence and in the presence of heparin (0.75 mg/ml) after 5 days, respectively. **(e)** Muramidase activity of HEWL (0.750 mg/ml) on *Micrococcus lisodectycus* at 540 nm (○) or after 5 min (●), 10 min (▲), 20 min (▼), 1 h (■) and 24 h (□) of HEWL:heparin after 5 days of preincubation and the control of heparin alone (△).**(f)** Leakage of DOPC:DOPA(8:2) SUV by HEWL preincubated with heparin at different time. See ESI

FTIR structural characterization of heparin-induced HEWL nanofibrils: in order to determine whether the heparin: HEWL interaction can lead the protein through the unfolding pathway to reach the fibrillar aggregate, we examine the infrared amide I´ band that absorbs at wave numbers ranging from 1600 to 1700 cm^{-1}, since this band is sensitive to study changes in protein folding processes in a dynamic way.[49] Moreover, this technique is able to distinguish between the ordered ß-sheet conformations in native proteins and insoluble ones from amyloid fibrils.[50] Figure 2a shows the deconvolved amide I´ spectra of HEWL in the absence or in the presence of heparin as a function of incubation time. The FTIR spectrum of monomeric HEWL has a dominant band at 1654 cm^{-1} which was assigned to the α-helix structure, while the band centered at 1649 cm^{-1} is due to the unordered regions. The presence of the two characteristic bands at 1632 and 1678 cm^{-1} corresponds to antiparallel β-sheet structure, while the components at 1657 cm^{-1} correspond to turns. The HEWL spectrum remained unchanged after 12 h of incubation at 37 °C (not shown). Upon addition of 3.75 mg/ml heparin, changes in the shape of the amide I´ were observed due to the presence of a new band located near 1612 cm^{-1} assigned to cross-ß structure. However, the overall fold of the protein remains the same. This data, together with the presence of cross-ß structure indicate that fibrils shown in Figure 1 are consistent with an amyloid-like supramolecular arrangement.[51] In order to understand better the changes taking place during the heparin-induced HEWL fibrillation, we performed the spectral deconvolution and curve fitting of the amide I´ band to obtain the individual Gaussian contributions of each element of secondary structure or quaternary structure. The results are shown in Figure 2b and 2c and Table 1. It is important to notice that data obtained from native HEWL fully agrees with previous FTIR analysis as well as form X-ray crystallographic analysis validating our curve analysis procedure.[52]

Considering the fact that the aggregation curves of Figure 1a and 1b almost did not show a lag time, and the overall structure of the Amide I' did not change after 1 h of heparin:HEWL incubation, it can be assumed that the polysaccharide acts as a real scaffolding of the fibril formation, offering an electrostatic surface where the protein molecules rapidly form aggregates. Therefore, heparin could act as a crowding surface, aligning and adjusting the HEWL conformation to the new physicochemical environment helping new inter-chain interactions.[53] In order to consider this possibility, we have determined the amounts of free heparin present after 5 days incubation with HEWL. After a thorough washing of the fibril, in order to remove any adsorbed heparin molecule, 0.46±0.02 mg heparin/mg HEWL were still present in the fibrils, representing 61% of the initial amount of heparin added to the solution. As a consequence the polysaccharide also forms part of the structure of the hybrid fibrils. This result agrees with previous work that has been described in systems, one where fluorescein-labeled heparin was incorporated into α-synuclein fibrils,[42] suggesting that heparin is integrated into the fibrils and is not just a catalyst for fibrillation.

Similar changes in the structural component of Amide I band were observed by Zou *et al*,[54] revealing also that the fibril-forming solution of HEWL has the capability to form fibrils and oligomers with distinct β-sheet configurations under different temperatures.

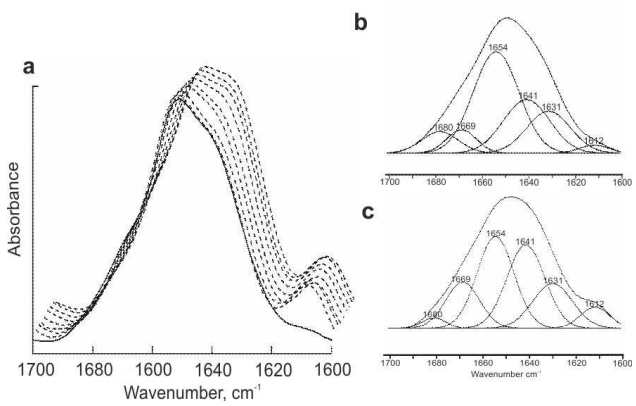

Figure 2 (a) Stacked spectra of deconvolved Amide I´ infrared spectra of 5 mg/ml of HEWL (solid line) and in the presence of 3.75 mg/ml of Hep after 30 min, 1h, 2h, 5h, 24h, 48h, 5 and 7 days at 37 °C of incubation (dashed lines). The spectra has been deconvolved with a half width of 18 and a K of 1,75. Amide I´ band decomposition of **(b),** HEWL and **(c),** HEWL: heparin after 5 days of 37 °C incubation. The spectrum in D_2O buffer showing the component bands, the envelope and, in dashed lines, the reconstruction of the amide I band from the components.

Table 1 [a]Band Position (cm^{-1}), structural assignment and [b]percentage area (%) corresponding to the components obtained after Curve Fitting the Amide I' band of the HEWL at 37 ºC in the presence and in the absence of heparin 0.750 mg/ml at different incubation times in D_2O medium.

Table I

Wavenumber [a] (cm^{-1})	Structural assignment	% amide I´area	
		-Hep	+Hep 5 days
1612	**Cross-β**	-	10
1631	**β-sheet**	**18**	17
1641	**Random coil**	**23**	26
1654	**α-helix**	**44**	33
1669	**β-turns**	**8**	9
1680	**β-sheet**[c]	**7**	5

[a]Band position (cm^{-1}), structural assignment and percentage of amide I´area (%) corresponding to the components obtained after curve fitting of the HEWL alone and in the presence of Hep after 5 days of incubation. [b]Antiparallel β-sheet high frequency component.

Molecular modeling of lysozyme-heparin interaction: HEWL was examined for heparin binding sites using a previously developed docking protocol.[43] Although a binding pocket for heparin was not evident, a favorable electrostatic interaction is expected to occur due to the high positive charge density on the protein surface and the negative charge arising from the sulfated groups in heparin (Figure 3a). The polyanionic-polycationic electrostatic interaction is responsible for the fast aggregation of HEWL in the presence of heparin as evidenced by the rapid increase in turbidity[55] or as was observed in second order light scattering assays (Figure 1b). Along with the increase in turbidity, there is a concomitant growth in the cross-ß structure formation, as monitored by thioflavin-T fluorescence intensity (Figure 1a). The formation of cross-ß structure without major changes in the secondary structure of the protein reported by infrared spectroscopy (Figure 2) might be explained by the interaction between ß-domains.[29] To test this hypothesis, we performed protein-protein docking studies of HEWL using pyDockWeb.[56] The docking poses were filtered for solutions compatible with the formation of cross-ß structure between the monomers. The putative HEWL dimers were evaluated for the presence of heparin binding pockets. Ten different putative HEWL:heparin complexes were obtained and subjected to molecular dynamic simulations. After 50 ns of simulation, three of the starting structures converged into the formation of stable protein-ligand complexes, and snapshots from the last 15 ns were used to estimate the relative binding affinities as described in material and methods. In the absence of heparin, the protein dimeric structures showed an unfavorable binding energy of 15 kcal/mol, due to the repulsion of the positive electrostatic fields arising from the HEWL monomers. This electrostatic repulsion could be counteracted by the binding of heparin. Indeed, binding of heparin in positively charged grooves at the putative dimer interface, greatly enhances the formation of the protein heparin complex, with a favorable binding energy of -25 kcal/mol for the ternary complex. By neutralizing the electrostatic repulsion between the HEWL monomers, heparin allows for the formation of hydrogen bonds between ß-strands in an anti-parallel pattern (Figure 3b). This model agrees with the observations derived from FT-IR measurements, in that it does not need major conformational rearrangement of the protein native fold. It should be also noticed that the time scale achievable through simulations, does not allow to model the whole range of conformational changes in protein upon heparin binding occurring in the minute to hour timescales. It is quite possible that the residues surrounding the ß-strands reorganize into a ß-sheet allowing the association of dimeric structures into larger protofibrils.

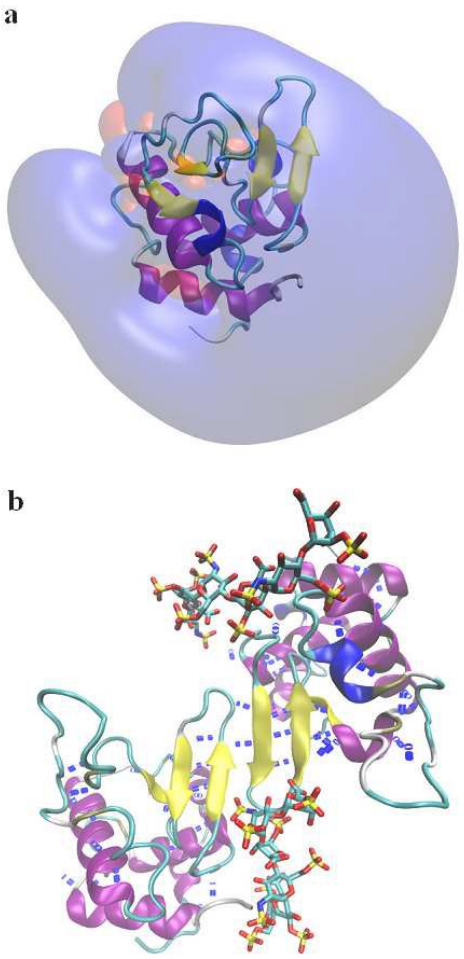

Figure 3 (a) Electrostatic isosurface potential at +1kTe (blue) and -1kTe (red) for HEWL (shown in cartoon representation). The potential was calculated by solving the non-linear adaptive Poisson–Boltzmann equation. **(b)** Model of the putative HEWL dimer (shown in cartoon) stabilized by heparin (licorice representation) bound to the basic residues at the protein surface. Hydrogen bonds are represented by blue dotted lines.

3.4 Photo-induced immobilization of lipase on the nanofibrils

In order to attach the intact lipase on the insoluble hybrid amyloid nanofibrils, we applied the photoinduced crosslinking of unmodified proteins (PICUP) method proposed by Fancy *et al.*[38] Briefly, it is based on the photo-induced electron-transfer quenching reaction produced after blue-light excitation of the ruthenium (II) tris-bipyridine complex $[Ru^{II}(bpy)_3]^{2+}$ in the presence of the electron acceptor persulfate anion $S_2O_8^{2-}$ to produce the oxidized $[Ru^{III}(bpy)_3]^{3+}$, the sulfate radical anion $SO_4^{\cdot-}$, and the non-reactive sulfate anion SO_4^{2-} (Scheme 1). Both $[Ru^{III}(bpy)_3]^{3+}$ and $SO_4^{\cdot-}$ species are potent one-electron oxidants capable of oxidizing available electron-rich amino acid residues generating side-chain radicals able to recombine to form covalent cross linked protein oligómers.[39, 57] During the global process the sensitizer $[Ru(bpy)_3]^{2+}$ is recovered and considering the molar excess of $S_2O_8^{2-}$ it can be considered that under photo-stationary conditions the concentration of protein radical precursors is nearly constant.[44] The involvement of aromatic aminoacid residues X (*e.g.* Tyr and Trp) in the formation of cross-linking bonds, *i.e.* $Prot_1$-X-X-$Prot_2$ (Scheme 1), can generate new chromophoric groups absorbing at >300 nm, as it is the case of di-tyrosine bridges formed by recombination of two side-chain tyrosyl radicals with distinctive absorption and fluorescence maxima approximately at 320 nm and 405 nm under neutral pH conditions, respectively.[58]

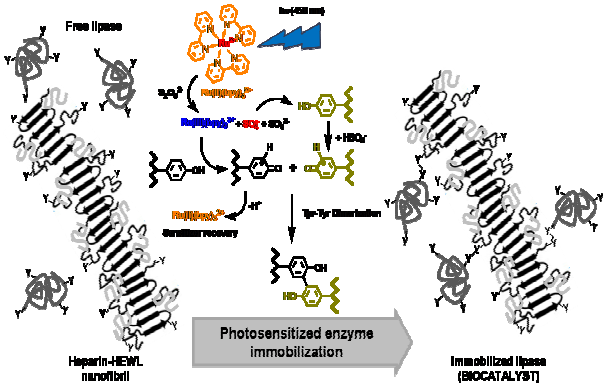

Scheme 1: pictorial representation of the photo-induced cross-linkingbetween free lipase and hybrid heparin-HEWL amyloid-like nanofibrils through formation of di-tyrosine bridges using $[Ru(bpy)_3]^{2+}/S_2O_8^{2-}$ as photosensitizing mixture. Docked heparin molecules are represented with light-gray lines. The photosensitized scheme reaction involving side-chain tyrosine residues of different proteins to produce the di-tyrosine cross-linking are represented in the center. This simplified scheme is not intended to represent the defined structure of the amyloid fibril. It shows the availability of Tyr side-chains in the regions which are not involved in the formation of cross-beta structure.

Figure 4a shows the effect of ascorbic acid on the kinetic profile of the absorbance change at 320 nm during the blue-light photolysis of $[Ru(bpy)_3]^{2+}/S_2O_8^{2-}$ of suspensions containing 1 mg/ml lipase and 1 mg/ml of amyloids nano-fibrils. In the absence of ascorbic acid, the absorbance increment during the initial ten minutes of photolysis suggests the formation of new chromophoric species. However, in the presence of 4 mM ascorbic acid, a well-known radical scavenger, the photosensitized reaction of the suspension produced no change in absorbance, confirming that the new chromophoric species are formed by photo induced radical-mediated steps as mentioned above. Figure 4b shows the emission spectra obtained by selective excitation at 295 nm of the suspension of lipase and amyloid nanofibrils before and after 20 min of blue-light photolysis of $[Ru(bpy)_3]^{2+}$ in the presence of $S_2O_8^{2-}$. Before photolysis, a blue-shifted protein emission spectra with maximum at 334 nm was observed (magenta solid line), suggesting the presence of partially buried Trp residues in the mixture,[59] in agreement with the secondary arrangement of the Trp residues of both HEWL and lipase proteins. On the other hand, after 20 min of blue-light photolysis and under identical excitation conditions, a new red-shifted and broader emission band was observed (blue solid line), suggesting the formation of new fluorophoric species during the photosensitization. In order to link these new fluorophores with the changes in absorbance produced at 320 nm during photosensitization, the supernatant and insoluble fractions of the photolyzed material were separated by centrifugation (see Experimental) and the emission spectrum with excitation at 320 nm was analyzed for both fractions. The soluble material (orange solid

line) showed much broader and red shifted emission than the re-suspended pellets (green solid line), suggesting a different nature of the side-chain fluorescent oxidation products after photosensitization. In the case of the re-suspended pellets the narrower emission spectrum with maximum at 405 nm is typical of di-tyrosine fluorophore at neutral pH,[58] as it was previously observed during the photosensitized formation of covalent oligomers of α-synuclein, an unfolded protein that contains four Tyr residues without Trp ones.[44] Therefore, it can be expected that after photosensitization treatment of the lipase and the hybrid nano fibrils, the insoluble material contains di-tyrosine bridges formed between surface accessible Tyr residues of both lipase and lysozyme component of the nano fibrils, allowing the covalent immobilization of the enzyme, as depicted in Scheme 1.

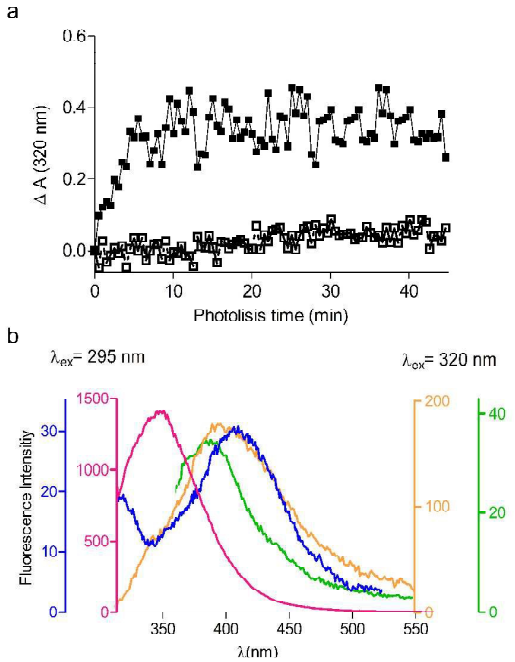

Figure 4 (a) Kinetic traces monitored by absorbance changes at 320 nm of blue-light photolyzed suspensions of 1 mg/ml lipase and 1 mg/ml of nanofibrils in the presence of 15 mM $[Ru(bpy)_3]^{2+}$ and 3 mM $S_2O_8^{2-}$ without (■) and with (□) the addition of 4 mM ascorbic acid. **(b)** Fluorescence emission spectra of the lipase-nanofibrils suspension observed by excitation at 295 nm before (magenta solid line) and after 20 min of blue-light photolysis (blue solid line), and by excitation at 320 nm of the re-suspended insoluble material (green solid line) and of the super natant material (orange solid line). See ESI

3.5 Effect of temperature and organic solvents on immobilized lipase stability via photo-induced immobilization onto a new hybrid nanomaterial

To prove the effective photo-induced immobilization of lipase on the amlyloid-like nanoscaffolds, and more importantly, if this insoluble material presents improved enzymatic activity we evaluated the residual activity of this material as a function of temperature and solvent conditions. Firstly, considering that, an improvement of the enzyme thermal stability is very desirable and attractive from the biotechnological point of view, the residual activity of either free or immobilized lipase was estimated after a pre-incubation during 1 h at various temperatures covering the range of 30 – 60 °C. As shown in Figure 5a, the photo-immobilized enzyme was relatively thermostable under our assays conditions. On the contrary, the residual activity of the free lipase declined as the incubation temperature increased having a more important effect above 45 ºC. The free enzyme lost 75 % (only retained 25 % of residual activity) of its activity after 1 h of incubation at 50 and 60 ºC, whereas the immobilized lipase retained 75 % of its initial activity after 1 h incubation under the same conditions. The lipase anchorage to the nanofibrils via a covalent bond leads to a decrease in the protein structure mobility at each anchorage point with a subsequent translation to the whole enzyme structure. As seen in other systems, this reduced freedom shields the enzyme from the denaturing effects of the environment. [8, 60] In fact, this decrease in flexibility overhelms the unfolding propensity of enzymes improving its activity.[61] Additionaly, an important increase of thermal stability was also observed in organophosphate hydrolase-amyloid complex but in this case, the immobilization was on amyloid fibrils generated from insulin using glutaraldehyde as crosslinking reagent.[62]

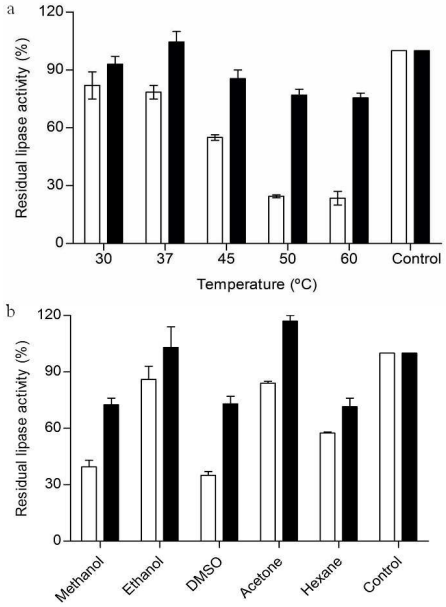

Figure 5 (a) Effect of temperature on residual lipase activity. **(b)** Effect of organic solvents on residual lipase activity using free lipase (white bars) or immobilized lipase (black bars). Remaining activity was compared with the control without incubation. Error bars represent the standard deviation calculated from at least three independent experiments.

Another important research line is the enzyme resistance towards organic solvents. This area is also very attractive, particularly in the field of biocatalytic resolution to synthetize building blocks for chiral agrochemical and pharmaceutical drugs. In addition, it is well known that lipases are diverse in their sensitivity to solvents, but there is a general agreement that water-miscible solvents are more destabilizing than water-immiscible ones. Related to this, the photo-immobilized enzyme showed an enhanced stability in the presence of water-miscible organic solvent such as methanol, ethanol, dimethyl sulfoxide and acetone (Figure 5b). As compared to the free enzyme, in the presence of methanol or ethanol the photo-immobilized lipase improved its residual activity by 33 % or nearly 20%, respectively, after 1h of pre-incubation at 37 °C. This

biocatalyst property could be useful in lipase catalyzed biodiesel production where methanol or ethanol tolerance is a key factor. [63] In addition, dimethyl sulfoxide which is widely used to disolve proteins, to a certain extent, slightly decreased the photo-immobilized residual lipase activity. The extremely high resistance of the photo-immobilized lipase in the presence of acetone under the same assays condition showing a residual lipase activity of 117% (117±4.24) was also specially interesting. Finally, the effect of hexane on either the free or the aqueous suspension of the photo-immobilized lipase was explored. In this case, the biocatalyst response included both inactivation by the interphase (interfacial toxicity) and inactivation by dissolved organic solvent (molecular toxicity). So, the biphasic system containing the photo-immobilized lipase showed a 71 % of residual activity after a pre-incubated for 1 h at 37°C.

Conclusions

The use of heparin as nucleation scaffold results in a simple strategy to obtain novel amyloid-like heparin-HEWL hybrid nanofibrils without any need to use high temperatures, low pHs or organic solvents, allowing this development to become a more viable and ecologically respectful process to produce suitable biomaterials as solid supports to improve biocatalysis.

By using a combination of spectroscopic, biophysical and biocomputational techniques, a molecular mechanism to explain the cross-ß structure formation induced by heparin without major changes in the HEWL tridimensional structure was proposed. Molecular Dinamic simulations showed that after docking of heparin into the protein, novel hydrogen bonds between ß-strands of different HEWL molecules appeared in an antiparallel pattern. This model meets the observations derived from FT-IR measurements. The orientation of the novel intermolecular ß-strands allows the formation of the classical amyloid nanofibrils ß-core resulting in the typical thermal stability. Furthermore, the present data provides an insight of the role that heparin (and other GAGs) can play in enhancing both formation and stabilization of amyloids.

In addition, hybrid heparin-HEWL nanofibrils have extra essential properties to be used as insoluble support for enzyme immobilization such as lack of biological activity and easiness to be functionalized due to the presence of solvent accessible amino acid residues which are not involved in the formation of the ß-core of the nanofibrils. Thus, results indicated that exposed Tyr residues in both nanofibril and lipase surfaces are suitable reactive groups for the application of the PICUP method using $[Ru(bpy)_3]^{2+}/S_2O_8^{2-}$ as photosensitizing mixture for a one-pot, fast and relatively efficient cross-linking process of enzyme immobilization through the formation of dityrosine bridges, which are easily detected and quantifiable by fluorescence spectroscopy. The cross-linked enzyme-nano-fibril system obtained showed enhanced solvent resistance and excellent performance at high temperature compared to the free lipase. Hence, this biocatalyst can be used in fine chemical processes such as enantiomer resolution and or biodiesel production.[64]

Thus, this photo-click chemical approach can be applied also to others amyloid-enzyme systems to develop different kinds of nano-biocatalysts. Although, further work is needed to achieve the best performance, and manufacture of amyloid nano-fibrils from cheaply available proteins, this research is a useful approach to design materials of commercial utility such as biocatalyst.

Experimental

Materials and methods

Materials: Hen Egg-White Lysozyme (HEWL, L-6876), lyophilized cells of *Micrococcus lysodeikticus* (A.T.C.C. 4698), lipase from porcine pancreas (L0382) was purchased from Fluka, heparin ammonium salt from intestinal mucosa, sephadex G-75, calcein, thioflavin T (ThT), p-nitrophenyl acetate (p-NPA), ruthenium (II) tris-bipyridine dichloride $Ru(bpy)_3Cl_2$, ammonium persulfate, proteinase K and 1,9-dimethyl-methylene blue (DMMB) were obtained from Sigma-Aldrich (St. Louis, MO) and used without further purification. Dioleylphosphatidylcholine (DOPC) and dioleylphosphatidic acid (DOPA) were obtained from Avanti Polar lipids and their purity controlled by thin layer chromatography (TLC).

Nanofibrils preparation: a 1 mg/ml HEWL solution was prepared in 20 mM HEPES, pH 7.4, centrifuged 30 min at 12000 x g and filtered with a 0.020 mm filter before every use to remove pre-aggregated material. Aggregation experiments were done by mixing 1 mg/ml of HEWL with 0.750 mg/ml heparin solutions tube and incubated at 37 ºC during 72 h. The obtained fibril suspension was pelleted by centrifugation and washed three times with freshly 20 mM HEPES, 200 mM NaCl pH 7.4 buffer aliquots to remove soluble material.

Aggregation kinetics of HEWL: To analyze the effect of heparin on amyloid fibril formation at 37 ºC, two types of experiments were conducted: ThT fluorescence intensity and second-order static scattering measurements. For fluorescence assay 0.1 mg/ml of HEWL solution mixed with 2 ml of 20 mM HEPES, pH 7.4, containing 25 µM ThT in the presence of different heparin concentration (e.g. 0.050, 0.060, 0.070, 0.075 and 0.1 mg/ml heparin). ThT fluorescence was registered with an ISS PC1 spectrofluorimeter (Champaign, IL, USA) with an excitation/emission wavelengths at 450 nm and 482 nm respectively.[41] The ThT fluorescence intensity growth kinetic at 482 nm was fitted to the exponential function $I_t = I_\infty[1 - \exp(-t/\tau_\beta)]$, where τ_β is the time at which the fluorescence intensity (I_t) reaches 63.2% of the maximal value (I_∞), the latter is proportional to the total amount of β-sheets conformations.

The second-order static scattering assay was performed by setting the excitation/emission wavelengths at 300 nm and 600 nm respectively. Intensity of HEWL solution, under the same conditions as described below, in the presence and in the absence of 0.075 mg/ml of heparin was recorded. Each reported data represents the average of at least three independent set of experiments.

Liposomal leakage test: the assay was performed according to Vechetti *et al* [65] Briefly to prepare DOPC:DOPA (8:2) SUV containing calcein trapped within, suitable amount of lipids were dried under nitrogen onto the wall of a Corex glass tube and sonicated with probe-type sonifier under nitrogen and controlled temperature. In order to separate calcein-loaded SUV from free dye a Sephadex G-75 was used. During incubation, changes in the fluorescence intensity of the different mixtures were monitored at λ exc=490 nm, λ em=510 nm[66] with the ISS PC1 spectrofluorimeter. Total dye release was completed by the addition of 0.1 vol % Triton X-100. The percentage of probe release was calculated as % Dye release=(IF-IB)/(IT-IB)×100, where IF, IT, and IB are the fluorescence intensity of the dye released by the protein, total dye released, and control blank.

Fourier transform infrared spectroscopy measurements: approximately 50 µl of sample containing 5 mg/ml of HEWL in deuterated buffer 20 mM HEPES, pD 7.4 was placed between two CaF_2 windows with 100 µm spacers in a thermostatized demountable liquid cell (Harrick Scientific, Ossining, NY). The spectra were recorded in a Nicolet 5700 spectrometer equipped

with a DTGS detector (Thermo Nicolet, Madison, WI). The sample chamber was permanently purged with dry air. Spectral blank subtraction, deconvolution, determination of band position and curve fitting of the original amide I band were performed as previously described by Arrondo *et al.*[51]

HEWL activity assays: the ability of lysozyme to produce the lysis of *M. lysodeikticus* cells was determined in 20 mM HEPES buffer (pH 7.4) at 25 °C according to Castro *et al*[47] by measuring the turbidity decreases of the cell suspension at 540 nm as a function of time with a Beckman DU 7500 UV-visible spectrophotometer.

Quantification of heparinin HEWL nanofibrils: the method that was used is described by Barbosa et al.[67] Briefly, amyloid suspensions were pre-treated with proteinase K before complexation with a 1,9-dimethyl-methylene blue (DMMB). After vigorous shaking for 30 min, samples were centrifuged (12000 x g, 10 min) in order to separate a precipitate of the sulfated polysaccharide-dye complex from thee supernatant containing all non-sulfated polysaccharidic compounds. Subsequently, the DMMB was released by complete dissociation of the insoluble complex by adding 500 µL of a decomplexant solution (50 mM sodium acetate buffer, pH 6.8 containing 4 M GuHCl 98% and 10% propan-1-ol). The DMMB absorbance on each sample at 650 nm was proportional to the amount of sulfated polysaccharide present in the sample, as calculated by comparison with a heparin calibration curve, (1-30 µg/mL of heparin).

Variable pressure scanning electron microscopy (VPSEM): approximately 50 ml of amyloid nanofibrils suspension at 1mg/ml concentration were put on a glass containing polylysine for an hour and then were fixed with a 2.5% glutaraldehyde in 0.1 M PBS (pH 7.4) for 15 minutes, afterwards they were washed thoroughly three-times with 0.1 M PBS for 15 minutes each one. Then the sample was dehydrated in graded series of alcohol each one for 15 minutes (25, 50, 75 and 100 % ethanol) mixture of 1:1 acetone:ethanol and pure acetone. Finally, it was dried up under critical point. EM analysis was performed using a LEO EVO 40-XVP scanning electron microscope (Bahia Blanca Argentina) at 7 kV with nominal magnifications of 30000×.

Protein-protein docking: docking poses for putative HEWL dimers were modeled using pyDockWeb server.[56] The NMR solution structure for HEWL was taken from the RCSB (entry 1E8L).[68] Solutions were filtered adding the participation of β-sheets in the formation of the interfaces as a restraint.

Lysozyme-heparin docking: the presence of heparin-binding sites on lysozyme monomer and putative dimers was studied using the software Autodock version 4.[69] The docking protocol and parameters have been described previously.[43] Briefly, input files were prepared using Autodock Tools.[69] Interaction scoring energies were calculated using a grid spacing of 0.375 spanning the whole protein surface. A total of 1000 configurations were generated using a Lamarckian genetic algorithm with all rotating bonds fixed. The candidate structures were clustered using a 2 Å threshold and the lowest energy cluster from the largest cluster was considered as the best docking solution.

Molecular dynamic simulations: all atom simulations were conducted using the NAMD package[70] with the CHARMm forcefield.[71] Topology and parameters for heparin were derived as previously reported.[72] Initial coordinates for the protein and heparin were derived from docking calculations. Each putative protein-ligand complex was solvated using a pre-equilibrated water box using the VMD[73] solvate plugin, and counter-ions were added to neutralize the system. During equilibration, the system was subjected to 10000 minimization steps followed by heating to 310 K for 1 ns using position restraints on CA atoms and further simulated for 10 ns without restraints. Production runs were simulated for each system for a total of 50 ns. Simulations were performed using periodic boundary conditions in the NPT ensemble. Non-bonded short-range interactions were treated using a 10Å cut-off, while electrostatic long-range interactions were treated using particle mesh Ewald algorithm.[74] Equations of motion were integrated using 1 fs timestep.

Estimation of binding affinities: binding energies for protein-protein and protein-ligand complexes were estimated from snapshots taken from the molecular dynamic simulation trajectories using the molecular mechanics Poisson-Boltzmann surface area (MM-PBSA) procedure.[75] Electrostatic contribution to the solvation energy was estimated through non-linear solution of the Poisson-Boltzmann equation using the APBS software package.[76] Atom radii and partial charges were taken from the CHARMm force field. The solvent and protein dielectric were set to 78 and 2 respectively, while the protein-solvent boundary was set using the molecular surface. Counter-ions were set to 20 mM and modeled implicitly. The non-polar contribution was calculated as a linear function of the solvent accessible surface of the molecule, using a 1.4 probe radius, and setting the gamma coefficient to 0.00542 kcal.mol^{-1}.Å^{-2}.

Lipase activity determination: lipase from porcine pancreas (Fluka) as a lyophilized power was used throughout this work. The reaction media containing 800 µl of 100 mM phosphate buffer (pH=7.0), 0.1% (wt/v) gum Arabic, 0.4% (w/v) Triton X-100,[77] and 100 µl of 1 mM p-NPA. The assay was conducted at 37 °C by the addition of either 100 µl of the immobilized lipase-amyloid nano-fibrils suspension or 100 µl of the free lipase solution, and the lipase activity was determined by release of *p*-nitrophenol (NP) as measured spectro photometrically at 405 nm.[77] One unit of hydrolytic activity was defined as the amount of biocatalyst that released 1 mmol of NP per minute under the given assay conditions.

Photoinduced cross-linking experiments: the covalent cross-linking between lipase and hybrid amyloid-like nanofibrils was performed by photosensitization reaction with 15 µM $[Ru(bpy)_3]^{2+}$in presence of 3 mM ammonium persulfate ($S_2O_8^{2-}$)[44,78] of 1.5 mg/ml of lipase and 1 mg/ml of amyloid-like nanofibrils in 1mL of 20 mM HEPES buffer (pH 7.4), 0.45% Triton XI00. The samples were placed in a cuvette holder with a magnetic stirrer, and irradiated with a 1 W blue LED (450 ± 27nm) for 15min, and the formation of photo-crosslinking products was monitored in-situ by UV-Vis spectrometry at 320 nm using a perpendicular analysing beam light from Ocean Optics USB2000 spectrometer system (Dunelin, FL, USA). Reaction was stopped by placing the sample protected from light and by addition of a small aliquot of concentrated β-mercaptoethanol and the biocatalyst was separated from the rest through washing by successive centrifuge for 4 minutes at 3000 × g. Steady-state fluorescence spectra of the starting and final materials were performed with a Hitachi F-2500 fluorometer (Kyoto, Japan).

Temperature effect on biocatalyst activity: one ml of either free or immobilized lipase was pre-incubated in 1 ml of 100 mM phosphate buffer (pH 7.0) for 1 h at different temperatures covering the range of 30–60 °C. The reaction mixture was shaken at 650 rpm. The remaining enzyme activity was then determined and compared with the control without pre-incubation.

Effect of water-miscible organic solvents on biocatalyst activity: one ml of either free or aqueous suspension of immobilized lipase was pre-incubated in a 1:1 ratio (v/v) with each organic solvent to be studied for 1 h at 37 °C. The reaction mixture was shaken at 650

rpm. The remaining enzyme activity was then determined and compared to the control without pre-incubation.

Effect of water-immiscible organic solvent on biocatalyst activity: to 500 µl of either free or aqueous suspension of immobilized lipase, 500 µl of hexane was added. The biphasic system was pre-incubated for 1 h at 37 °C. The reaction mixture was shaken at 650 rpm. The aqueous phase was sampled, and the remaining enzyme activity was then determined and compared to the control without pre-incubation.

Acknowledgements

We thank to R. A. Mignone (INBIONATEC) for technical assistance. This work was supported by the following Argentine research grants PIP12-0374, PICTO-UNSE-12-013, PIP 339 and PIP 0183 (CONICET), PIUNT E548/3 (UNT), PICT 2011- 2158 and PICT 2012- 2882 (FONCyT), PIUNT D541 (UNT) and Instituto de Desarrollo Productivo de Tucumán (IDEP). Computer power was gently provided by Centro Nacional de Supercomputação (CESUP), at Universidade Federal do Rio Grande do Sul (UFRGS).

Notes and references

1. J. C. Santos, N. Rueda, L. R. Goncalves and R. Fernandez-Lafuente, *Enzyme Microb Technol*, 2015, **77**, 1-7.
2. A. G. Cunha, M. D. Besteti, E. A. Manoel, A. A. T. da Silva, R. V. Almeida, A. B. C. Simas, R. Fernandez-Lafuente, J. C. Pinto and D. M. G. Freire, *Journal of Molecular catalysys B: Enzymatic*, 2014, **100**, 59-67.
3. N. Miletic, A. Nastasovic and K. Loos, *Bioresour Technol*, 2012, **115**, 126-135.
4. J. K. Poppe, R. Fernandez-Lafuente, R. C. Rodrigues and M. A. Ayub, *Biotechnol Adv*, 2015, **33**, 511-525.
5. A. S. de Miranda, L. S. Miranda and R. O. de Souza, *Biotechnol Adv*, 2015, **33**, 372-393.
6. B. Brena, P. Gonzalez-Pombo and F. Batista-Viera, *Methods Mol Biol*, 2013, **1051**, 15-31.
7. F. Lopez-Gallego, G. Fernandez-Lorente, J. Rocha-Martin, J. M. Bolivar, C. Mateo and J. M. Guisan, *Methods Mol Biol*, 2013, **1051**, 59-71.
8. M. L. Verma, M. Naebe, C. J. Barrow and M. Puri, *PLoS One*, 2013, **8**, e73642.
9. I. Deveci, Y. I. Dogac, M. Teke and B. Mercimek, *Appl Biochem Biotechnol*, 2014, DOI: 10.1007/s12010-014-1321-4 [doi].
10. D. Goswami, J. K. Basu and S. De, *Crit Rev Biotechnol*, 2013, **33**, 81-96.
11. J. Ge, D. Lu, Z. Liu and Z. Liu, *Biochemical Engineering Journal*, 2009, **44**, 53-59.
12. C. M. Dobson, *Nature*, 2003, **426**, 884-890.
13. S. L. Gras, A. K. Tickler, A. M. Squires, G. L. Devlin, M. A. Horton, C. M. Dobson and C. E. MacPhee, *Biomaterials*, 2008, **29**, 1553-1562.
14. F. Chiti and C. M. Dobson, *Annu Rev Biochem*, 2006, **75**, 333-366.
15. R. Nelson, M. R. Sawaya, M. Balbirnie, A. O. Madsen, C. Riekel, R. Grothe and D. Eisenberg, *Nature*, 2005, **435**, 773-778.
16. A. T. Petkova, R. D. Leapman, Z. Guo, W. M. Yau, M. P. Mattson and R. Tycko, *Science*, 2005, **307**, 262-265.
17. C. Goldsbury, P. Frey, V. Olivieri, U. Aebi and S. A. Muller, *J Mol Biol*, 2005, **352**, 282-298.
18. S. Hess, S. L. Lindquist and T. Scheibel, *EMBO Rep*, 2007, **8**, 1196-1201.
19. N. M. Kad, S. L. Myers, D. P. Smith, D. A. Smith, S. E. Radford and N. H. Thomson, *J Mol Biol*, 2003, **330**, 785-797.
20. F. Bemporad and F. Chiti, *FEBS Lett*, 2009, **583**, 2630-2638.
21. F. Chiti and C. M. Dobson, *Nat Chem Biol*, 2009, **5**, 15-22.
22. M. R. Sawaya, S. Sambashivan, R. Nelson, M. I. Ivanova, S. A. Sievers, M. I. Apostol, M. J. Thompson, M. Balbirnie, J. J. Wiltzius, H. T. McFarlane, A. O. Madsen, C. Riekel and D. Eisenberg, *Nature*, 2007, **447**, 453-457.
23. F. Meersman and C. M. Dobson, *Biochim Biophys Acta*, 2006, **1764**, 452-460.
24. S. Mankar, A. Anoop, S. Sen and S. K. Maji, *Nano Rev*, 2011, **2**.
25. J. F. Smith, T. P. Knowles, C. M. Dobson, C. E. Macphee and M. E. Welland, *Proc Natl Acad Sci U S A*, 2006, **103**, 15806-15811.
26. S. M. Pilkington, S. J. Roberts, S. J. Meade and J. A. Gerrard, *Biotechnol Prog*, 2010, **26**, 93-100.
27. A. M. C. N. R. Rao, A. K. Cheetham, ed., *Nanomaterials Chemistry. Recent Developments and New Directions*, Wiley-VCH Verlag, Weinheim,, 2007.
28. I. Cherny and E. Gazit, *Angew Chem Int Ed Engl*, 2008, **47**, 4062-4069.
29. D. R. Booth, M. Sunde, V. Bellotti, C. V. Robinson, W. L. Hutchinson, P. E. Fraser, P. N. Hawkins, C. M. Dobson, S. E. Radford, C. C. Blake and M. B. Pepys, *Nature*, 1997, **385**, 787-793.
30. M. B. Pepys, P. N. Hawkins, D. R. Booth, D. M. Vigushin, G. A. Tennent, A. K. Soutar, N. Totty, O. Nguyen, C. C. Blake, C. J. Terry and et al., *Nature*, 1993, **362**, 553-557.
31. L. A. Morozova-Roche, J. Zurdo, A. Spencer, W. Noppe, V. Receveur, D. B. Archer, M. Joniau and C. M. Dobson, *J Struct Biol*, 2000, **130**, 339-351.
32. M. F. Mossuto, A. Dhulesia, G. Devlin, E. Frare, J. R. Kumita, P. P. de Laureto, M. Dumoulin, A. Fontana, C. M. Dobson and X. Salvatella, *J Mol Biol*, 2010, **402**, 783-796.
33. W. Liu, J. M. Prausnitz and H. W. Blanch, *Biomacromolecules*, 2004, **5**, 1818-1823.
34. Y. Yonezawa, S. Tanaka, T. Kubota, K. Wakabayashi, K. Yutani and S. Fujiwara, *J Mol Biol*, 2002, **323**, 237-251.
35. B. A. Vernaglia, J. Huang and E. D. Clark, *Biomacromolecules*, 2004, **5**, 1362-1370.
36. N. Sarkar, M. Kumar and V. K. Dubey, *Biochimie*, 2011, **93**, 962-968.
37. H. Zhao, E. K. Tuominen and P. K. Kinnunen, *Biochemistry*, 2004, **43**, 10302-10307.
38. D. A. Fancy and T. Kodadek, *Proc Natl Acad Sci U S A*, 1999, **96**, 6020-6024.
39. L. G. Herman, S.; Defrancq, E.; Mesmaeker, A. K. D. , *J. Phys. Org. Chem*, 2008, **21**, 670-681.
40. H. J. Nandivada, X., *Advanced Materials* 2007, **19**, 2197-2208.
41. H. LeVine, 3rd, *Methods Enzymol*, 1999, **309**, 274-284.

42. J. A. Cohlberg, J. Li, V. N. Uversky and A. L. Fink, *Biochemistry*, 2002, **41**, 1502-1511.
43. C. M. Torres-Bugeau, C. L. Avila, R. Raisman-Vozari, D. Papy-Garcia, R. Itri, L. R. Barbosa, L. M. Cortez, V. L. Sim and R. N. Chehin, *J Biol Chem*, 2012, **287**, 2398-2409.
44. C. D. Borsarelli, L. J. Falomir-Lockhart, V. Ostatna, J. A. Fauerbach, H. H. Hsiao, H. Urlaub, E. Palecek, E. A. Jares-Erijman and T. M. Jovin, *Free Radic Biol Med*, 2012, **53**, 1004-1015.
45. E. A. Grula and S. E. Hartsell, *J Bacteriol*, 1954, **68**, 171-177.
46. G. F. Vechetti, B. F. de Arcuri, E. Posse, J. L. Arrondo and R. D. Morero, *Mol Membr Biol*, 1997, **14**, 137-142.
47. F. Castro, A. Rodríguez, G. Juárez and F. Fernández, *Acta zoológica lilloana*, 2009, **53** 49-56.
48. E. Posse, B. F. De Arcuri and R. D. Morero, *Biochim Biophys Acta*, 1994, **1193**, 101-106.
49. J. L. Arrondo, A. Muga, J. Castresana and F. M. Goni, *Prog Biophys Mol Biol*, 1993, **59**, 23-56.
50. G. Zandomeneghi, M. R. Krebs, M. G. McCammon and M. Fandrich, *Protein Sci*, 2004, **13**, 3314-3321.
51. J. L. Arrondo, J. Castresana, J. M. Valpuesta and F. M. Goni, *Biochemistry*, 1994, **33**, 11650-11655.
52. C. C. Blake, G. A. Mair, A. C. North, D. C. Phillips and V. R. Sarma, *Proc R Soc Lond B Biol Sci*, 1967, **167**, 365-377.
53. C. M. Torres-Bugeau, C. D. Borsarelli, C. J. Minhak and R. N. Chehin, *Curr Protein Pept Sci*, 2011, DOI: CPPS-109 [pii].
54. Y. Zou, Y. Li, W. Hao, X. Hu and G. Ma, *J Phys Chem B*, 2013, **117**, 4003-4013.
55. S. J. Wood, B. Maleeff, T. Hart and R. Wetzel, *Journal of molecular biology*, 1996, **256**, 870-877.
56. B. Jimenez-Garcia, C. Pons and J. Fernandez-Recio, *Bioinformatics*, 2013, **29**, 1698-1699.
57. B. C. Gau, H. Chen, Y. Zhang and M. L. Gross, *Anal Chem*, 2010, **82**, 7821-7827.
58. D. A. Malencik and S. R. Anderson, *Amino Acids*, 2003, **25**, 233-247.
59. J. R. Lakowicz., *Journal*, 2006.
60. E. Taqieddin and M. Amiji, *Biomaterials*, 2004, **25**, 1937-1945.
61. R. A. Sheldon and S. van Pelt, *Chem Soc Rev*, 2013, **42**, 6223-6235.
62. J. K. Raynes, F. G. Pearce, S. J. Meade and J. A. Gerrard, *Biotechnol Prog*, 2011, **27**, 360-367.
63. K. Nie, F. Xie, F. Wang and T. Tan, *Journal of Molecular Catalysis B: Enzymatic*, 2006, **43**, 142-147.
64. *Argentina Pat.,* 2014.
65. G. F. d. A. Vechetti, B. F. Posse, E. Arrondo, J. L.Morero, R. D., *Mol Membr Biol*, 1997, **14**, 137-142.
66. D. A. Kendall and R. C. MacDonald, *J Biol Chem*, 1982, **257**, 13892-13895.
67. I. Barbosa, S. Garcia, V. Barbier-Chassefiere, J. P. Caruelle, I. Martelly and D. Papy-Garcia, *Glycobiology*, 2003, **13**, 647-653.
68. H. Schwalbe, S. B. Grimshaw, A. Spencer, M. Buck, J. Boyd, C. M. Dobson, C. Redfield and L. J. Smith, *Protein Sci*, 2001, **10**, 677-688.
69. G. M. Morris, R. Huey, W. Lindstrom, M. F. Sanner, R. K. Belew, D. S. Goodsell and A. J. Olson, *J Comput Chem*, 2009, **30**, 2785-2791.
70. J. C. Phillips, R. Braun, W. Wang, J. Gumbart, E. Tajkhorshid, E. Villa, C. Chipot, R. D. Skeel, L. Kale and K. Schulten, *J Comput Chem*, 2005, **26**, 1781-1802.
71. A. D. Mackerell, Jr., M. Feig and C. L. Brooks, 3rd, *J Comput Chem*, 2004, **25**, 1400-1415.
72. S. S. Mallajosyula, O. Guvench, E. Hatcher and A. D. Mackerell, Jr., *J Chem Theory Comput*, 2012, **8**, 759-776.
73. W. Humphrey, A. Dalke and K. Schulten, *J Mol Graph*, 1996, **14**, 33-38, 27-38.
74. T. Darden, D. York and L. Pedersen, *The Journal of Chemical Physics*, 1993, **98**, 10089.
75. P. A. Kollman, I. Massova, C. Reyes, B. Kuhn, S. Huo, L. Chong, M. Lee, T. Lee, Y. Duan, W. Wang, O. Donini, P. Cieplak, J. Srinivasan, D. A. Case and T. E. Cheatham, 3rd, *Acc Chem Res*, 2000, **33**, 889-897.
76. N. A. Baker, D. Sept, S. Joseph, M. J. Holst and J. A. McCammon, *Proc Natl Acad Sci U S A*, 2001, **98**, 10037-10041.
77. U. K. Winkler and M. Stuckmann, *J Bacteriol*, 1979, **138**, 663-670.
78. D. A. D. Fancy, C. Kim, K. Xie, Y. Holdeman, T. Amini, F. Kodadek, T., *Chem Biol*, 2000, **7**, 697-708.

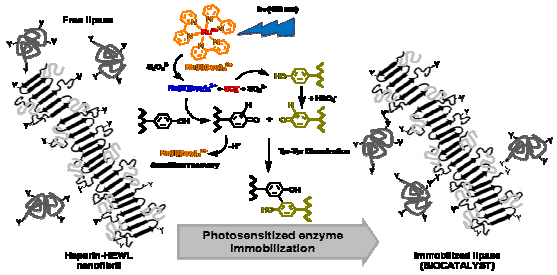

Photoimmobilization of enzymes on an amyloid-like fibrilar scaffold